Available online at www.eccomasproceedia.org
Eccomas Proceedia COMPDYN (2023) 497-510

ECCOMAS
Proceedia

COMPDYN 2023
9th ECCOMAS Thematic Conference on
Computational Methods in Structural Dynamics and Earthquake Engineering
M. Papadrakakis, M. Fragiadakis (eds.)
Athens, Greece, 12-14 June 2023

SHEAR RETROFITTING OF REINFORCED CONCRETE T-BEAMS USING CARBON FIBER-REINFORCED POLYMER (FRP) ROPES AND U-SHAPED SHEETS - TESTS AND FRP DEBONDING FAILURE IDENTIFICATION

Adamantis G. Zapris[1], Violetta K. Kytinou[1], George M. Sapidis[1], Constantin E. Chalioris[1], Chris G. Karayannis[2]

[1] Laboratory of Reinforced Concrete and Seismic Design of Structures, Department of Civil Engineering School of Engineering, Democritus University of Thrace, Xanthi 67100, Greece
e-mail: {azapris, vkytinou, gsapidis, chaliori}@civil.duth.gr

[2] Laboratory of Reinforced Concrete and Masonry Structures, Department of Civil Engineering School of Engineering, Aristotle University of Thessaloniki, Thessaloniki 54124, Greece
e-mail: karayannis@civil.auth.gr

Abstract

Seismic shear failure in Reinforced Concrete (RC) structures is characterized by brittle diagonal cracking. Old RC buildings have low shear capacities due to inadequate transverse reinforcement. To address this issue, Externally Bonded Fiber Reinforced-Polymer (EB-FRP) sheets are a promising strengthening technique, but their effectiveness depends on the bond characteristics between the FRP and concrete surface. U-jacketed EB-FRP sheet applications have resulted in premature debonding failures, leading to the proposal of alternative strengthening techniques such as Near Surface Mounted (NSM) or Embedded Through-Section (ETS) FRP ropes. Also, identifying the state of health in FRP-retrofitted RC infrastructures is critical to prevent further deterioration and collapse, particularly in seismic-prone regions. To address this challenge, this study constructed and tested three large-scale shear-critical RC beams with T-shaped cross-sections, two of which were strengthened with carbon FRPs. The beams were retrofitted with EB-FRP sheets and FRP ropes. During testing, a novel Electro-Mechanical Admittance (EMA) based Structural Health Monitoring (SHM) system was implemented using smart Piezoelectric lead Zirconate Titanate (PZT) transducers/actuators to vibrate and monitor the retrofitted beams in real-time. This study provides valuable insights into the effectiveness of various shear retrofitting techniques and the use of SHM systems to ensure the safety of FRP-retrofitted RC infrastructures.

Keywords: Shear, Retrofitting, Fiber Reinforced-Polymer (FRP), FRP Rope, Structural Health Monitoring (SHM), Piezoelectric Lead Zirconate Titanate (PZT) Transducers

ISSN:2623-3347
Peer-review under responsibility of the organizing committee of COMPDYN 2023.
doi: 10.7712/120123.10416.20742

1 INTRODUCTION

Seismic activity poses a significant threat to the structural integrity of Reinforced Concrete (RC) buildings. The resulting shear failure in RC structures is a catastrophic event that can lead to partial or complete collapse. The brittle nature of this type of failure is marked by extensive diagonal cracking, which can quickly propagate and compromise the entire structure. It is particularly concerning that many older RC buildings have deficient transverse reinforcement configurations that make them even more vulnerable to shear failure [1]. These buildings may have been constructed before the development of modern seismic design codes or may have been designed with inadequate attention to seismic resilience. The use of Shear retrofitting techniques, such as Externally Bonded Fiber Reinforced-Polymer (EB-FRP) sheets, has emerged as an effective strategy for enhancing the strength and ductility of vulnerable RC structural members [2]. The application of EB-FRP sheets on the surface of RC structures increases the shear resistance of the components, thereby reducing the likelihood of failure during a seismic event [3, 4]. This method of shear retrofitting is particularly appealing because it is relatively easy to install and can be applied to existing structures without major structural alterations [5].

This approach is characterized by the application of FRP sheets to the external surfaces of a structure, allowing for increased strength and durability. However, the success of this method is dependent on the bond characteristics between the FRP and the concrete surface [6, 7]. In some cases, premature debonding failures have been reported, particularly in applications that involve U-jacketed EB-FRP sheets on typical T-shaped beams [8, 9]. To address this issue, alternative strengthening methods have been proposed, such as Near Surface Mounted (NSM) or Embedded Through-Section (ETS) FRP ropes [10-12]. These techniques can provide increased bond strength between the FRP and the concrete, reducing the likelihood of premature debonding failures. This is because the FRP material is embedded into the concrete and anchored at both ends providing an efficient load transfer mechanism, rather than just being attached to the surface [13, 14]. Recently, a few studies have been conducting indicating the promising results of the use of FRP ropes as strengthening method in RC beams and Joints however further investigation is necessary to fully understand their effectiveness and potential drawbacks of these techniques [15, 16]. Additionally, continued research is needed to identify and address any potential issues or limitations associated with the application in real structures.

Despite the promising results of FRP retrofitting in enhancing the shear capacity of vulnerable RC structures, it is crucial to ensure that the long-term performance of retrofitted structures is monitored and maintained [17, 18]. Therefore, a critical challenge is the development of effective state-of-health monitoring techniques that can detect potential failures in FRP-retrofitted RC infrastructures promptly [19-21]. These techniques can help to prevent shear critical or FRP debonding failures that may lead to further deterioration and sudden collapse, especially in regions with high seismic activity [22-24]. In this context, the implementation of advanced monitoring systems, such as structural health monitoring (SHM) using sensors can provide continuous monitoring and evaluation of the performance and integrity of FRP-retrofitted RC structures, allowing for early detection of potential failures and timely interventions to mitigate the risk of catastrophic events [25, 26].

In light of these challenges, in this study three large-scale shear-critical RC beams with T-shaped cross-sections were constructed, two of which were strengthened with carbon FRPs and tested. To enhance their shear capacity, the T-beams were strengthened with either EB-FRP sheets applied to the three sides of the beam, serving as external U-shaped transverse reinforcement, or with FRP ropes installed on the perimeter of the web, serving as NSM rein-

forcement against shear. In addition, a novel remotely controlled Electro-Mechanical Admittance (EMA) based Structural Health Monitoring (SHM) system with smart piezoelectric lead zirconate (PZT) sensors [27-29], was deployed during testing. The PZT sensors were mounted on the FRP ropes and sheets of the retrofitted beams in predetermined locations, respectively. The SHM devices simultaneously monitored the signal of the same PZT transducers/sensors and transmitted their voltage frequency response, after processing wirelessly and in real-time, to facilitate continuous identification of potential damage and the condition of the FRPs. Based on the experimental results of this work, valuable conclusions concerning the applied shear retrofitting techniques were drawn, with the forthcoming debonding failure of the FRP materials also being examined and quantified using the proposed SHM technique and statistical analysis derived from different damage indices.

2 EXPERIMENTAL PROGRAM

2.1 Description of Specimens

Three RC beams of L = 2.0 m length were tested as part of the experimental program. The beams had a T-shaped cross-section to replicate the slab existence situation. The height to width ratio of the web cross-section was 300/150 mm, whereas it was 50/300 mm for the slab. The beams were constructed with the intention that their flexural strength exceeded their shear strength. The shear span of the beams lacked transverse reinforcement, whereas their longitudinal reinforcement consisted of 4Ø16 mm at the bottom of the web cross-section and 2Ø14 mm at the top. In addition, an extra 2Ø10 mm of longitudinal reinforcement was added to the slab region. (Figure 1).

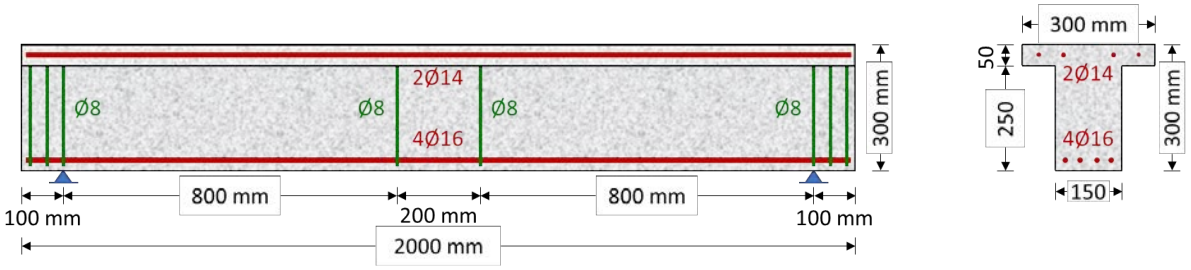

Figure 1: Specimen dimensions and reinforcements arrangement.

Among the three specimens tested, one acted as the reference specimen (S0) while the other two specimens (S0-U and S0-RF) underwent shear strengthening, The S0-U specimen was strengthened by externally bonding strips of FRP sheets around the beam's web, following a U-shape configuration (Figure 2a). For this type of strengthening, a single layer of FRP sheet strips, with the fiber direction perpendicular to the beam's longitudinal axis, was applied. The strips had a width of l_s = 160 mm and were placed at s_s = 160 mm distances around the web. On the other hand, the S0-RF specimen underwent shear strengthening using FRP ropes. The ropes were placed in grooves drilled around the beam web and in the upper part of the slab, with holes in the slab allowing for a full wrapping of the cross-section. The ropes were placed per l_s = 160 mm distance, with a direction perpendicular to that of the longitudinal axis of the beam (Figure 2b). The geometric percentage of the two reinforcements was approximately equal, with $\rho_{f,s}$ = 0.22% for FRP sheet strips and $\rho_{f,r}$ = 0.23% for FRP ropes.

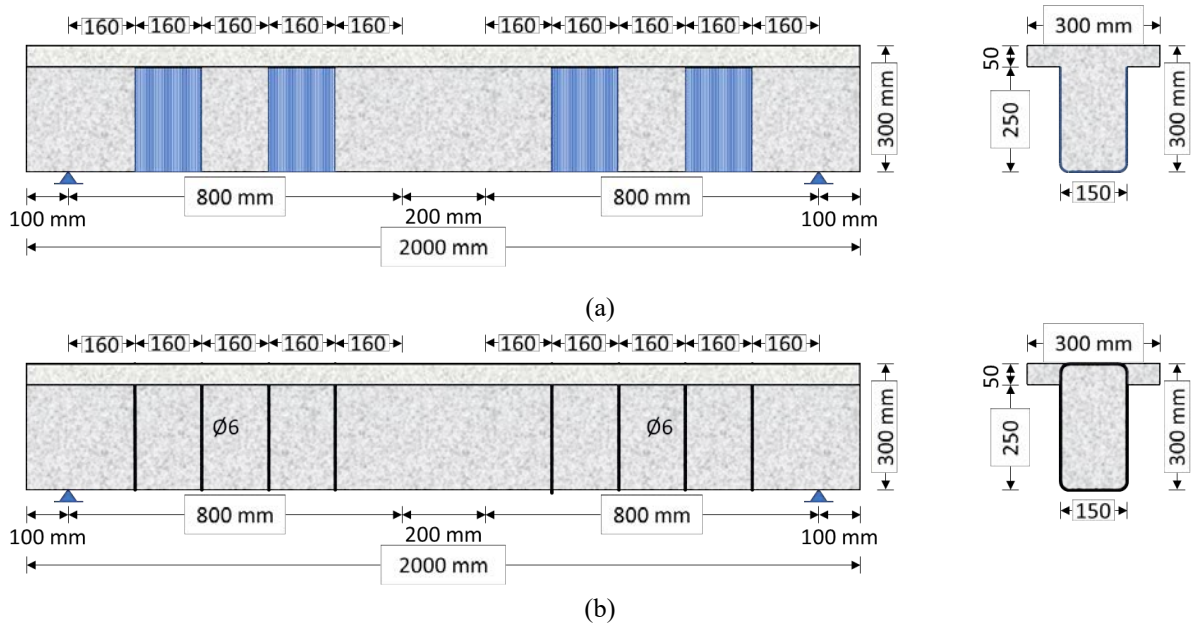

Figure 2: Beam's strengthening: (a) with EB-FRP sheet strips around the web (S0-U) and (b) with FRP ropes with the application of NSM technic.

2.2 Strengthening Application Procedure

For beam S0-U, which was strengthened with FRP sheets, the sheet application positions were marked in advance, and then the concrete's outer layer was removed using a suitable instrument. The edges of the web section were curved to avoid local fracture of the FRP sheets. The area was cleaned thoroughly using compressed air to remove dust and other debris. After the FRP sheets were carefully measured and cut to the desired size, the surface of the beam was coated with epoxy resin, and the impregnation resin was applied to the sheets meticulously, adhering to the manufacturer's instructions. Finally, a special roller was used to apply the sheets to the designated surface of the beam.

The beam S0-RFwas strengthened using unidirectional carbon fiber bundles, known as FRP ropes. First, using a suitable tool, the notches (grooves) were created in the area of the web of the beam and as well the slab (Figure 3a). The notches were then widened using a drilling machine (Figure 3b). Also, using the drilling machine, from the beam to the slab direction, holes were drilled in the slab to join the notches of each side (Figure 3c). Both the edges of the beam body and the points of connection of the holes with the notches, in the upper part of the beam, were curved with special attention to avoid local fracture of the fibers (Figure 3d). After the end of the operations, the areas were thoroughly cleaned using compressed air to remove dust and debris. The FRP ropes were then cut to the desired length. One of their ends, after being impregnated with the appropriate resin, was placed in the notches in the upper part of the beam, where the anchoring resin had previously been applied in spots (Figure 3e). The fibers were left undisturbed for a day until the resins developed some strength. Then, using a roller, the fibers were wetted with the impregnation resin. Simultaneously with the impregnation of the fibers, the inner surfaces of the holes and notches were smeared with the anchoring resin (Figure 3f). The impregnated rope was then placed inside the notches (Figure 3g). Special care was taken to avoid any damage to the fibers during impregnation and rope placement. The rest of the notches and holes were then filled with the anchoring resin (Figure 3h). Finally, a small constant load was applied to the free end of the cords to ensure that the fibers are fully stretched (Figure 3i).

Figure 3: Strengthening application procedure of S0-RF beam: (a) Creating the notches (web, slab), (b) using a drilling machine to widen the notches of the web and the slab, (c) using a drilling machine to drill holes in the slab and connect the notches on either side, (d) curving of the web edges of the upper side of the beam (connection point of holes and notches) to prevent local failure., (e) impregnation of rope end and placing it in the notches of the upper part of the beam (slab) after they have been coated with resin (anchorage area), (f) Coating the holes and notches all around the web with resin and impregnation of the rope, (g) placing of the FRP rope in the notches, (h) filling the holes and notches with resin and (i) application of small load on the ropes' free ends to "stretch" the fibers.

2.3 Materials

To obtain the mechanical characteristics of the concrete, cylindrical specimens were fabricated during the concrete casting process. The specimens were then subjected to compressive and split tensile tests, resulting in an average compressive strength of f_{cm} = 44.2 MPa and an average tensile strength of f_{ctm} = 3.1 MPa, based on the analysis of 12 concrete cylinders. The longitudinal and transverse reinforcements used in all beams were of B500C class.

The beam S0-U underwent a strengthening process using a unidirectional carbon fiber fabric (SikaWrap®-600 C). The manufacturer's specifications indicated that the sheet's nominal thickness, average tensile strength, average modulus of elasticity, and elongation at rupture were 0.331 mm^2, 3000 N/mm^2, 225 kN/mm^2, and 1.33%, respectively. The sheet was impregnated with a two-component thixotropic and epoxy resin (Sikadur®-300) to adhere to the beam's surface. The resin's rupture elongation was 0.9%, its tensile strength was 30 N/mm^2, and its elastic modulus was 4500 N/mm^2.

The strengthening of the S0-RF beam was performed using unidirectional carbon fibers (SikaWrap® FX-50C). According to the manufacturer's specifications, after the impregnation procedure, the CFRP rope has an area of about 78 mm^2 (dry fiber cross-section >28 mm^2), a tensile strength of 2000 N/mm^2, a modulus of elasticity of 230 kN/mm^2 and an ultimate strain of 0.87 %.

The resin used to impregnate the fibers (Sikadur®-52 Injection LP) has a compressive strength of 34 N/mm^2, a tensile strength of 24 N/mm^2 and a tensile modulus of elasticity of 1100 N/mm^2. A two-component, thixotropic and epoxy resin (Sikadur®-330) was used to embed and anchor the fibers into the grooves. The tensile strength, the modulus of elasticity and the rupture elongation of the resin are 30 N/mm^2, 4500 N/mm^2 and 0.9%, respectively.

2.4 Experimental Setup and Instrumentation

The specimens were positioned on two metal rods 100 mm from each end of the beam. In displacement control mode, a load rate of 0.01 mm/s was applied via two metal rods placed

on either side of the beam's middle. To measure displacements at the expected position of maximum moment, two linear variable differential transducers (LVDT) were installed at the bottom of the beam, one on the front side and one on the back side. Furthermore, an LVDT was positioned at the bottom of each support to monitor any potential movements (Figure 4).

Figure 4: Test set-up.

This study used an electromechanical impedance (EMI) method in the custom-built, wireless SHM and damage evaluation system. A real-time EMI measurement was implemented using PZT patches through an advanced device (WiAMS). Furthermore, the competence of the PZT patches to act as transducers when subjected to an amplified harmonic excitation voltage signal and concurrently to operate as sensors acquiring the reflected waves concerning the electrical impedance in response to a frequency range deriving benefit from the merits of the piezoelectric phenomenon was also exploited.

Four PZT transducers, with dimensions 10 × 10 mm, were externally epoxy-bonded to the surfaces of the FRP sheets and ropes for each specimen accordingly. In order to monitor the bonding degradation of externally placed FRP reinforcement, two cables were connected to the PZT's patch poles. A series of measurements via the wireless system WiAMS in a frequency range of 10 to 250 kHz in each damage state.

3 RESULTS

3.1 Experimental Response of the Beams

This section provides a succinct overview of the behavior of each beam by outlining the cracking progression and ultimate failure mode. Additionally, an analysis and discussion of the load versus deflection diagram at the midpoint of the beams is included to facilitate comprehension of their response.

In the initial loading stages, the S0 specimen (reference specimen), demonstrated an elastic response up to a 50 kN load. With a slight increase in load, the first flexural cracks emerged in the midspan of the beam, and as the load continued to rise, a few flexural cracks also developed in the shear spans. The first shear crack appeared in the left shear span at a load of 130 kN, accompanied by another in the right shear span and a minor reduction in the beam’s strength. The length and width of the right shear span shear crack gradually increased, and the

fracture expanded into the slab area. The beam ultimately failed because of the widening of the slab crack, which occurred at 143 kN. To acquire a better understanding of the beam's response, a load versus deflection diagram at the beam's midspan is provided and discussed (Figure 5).

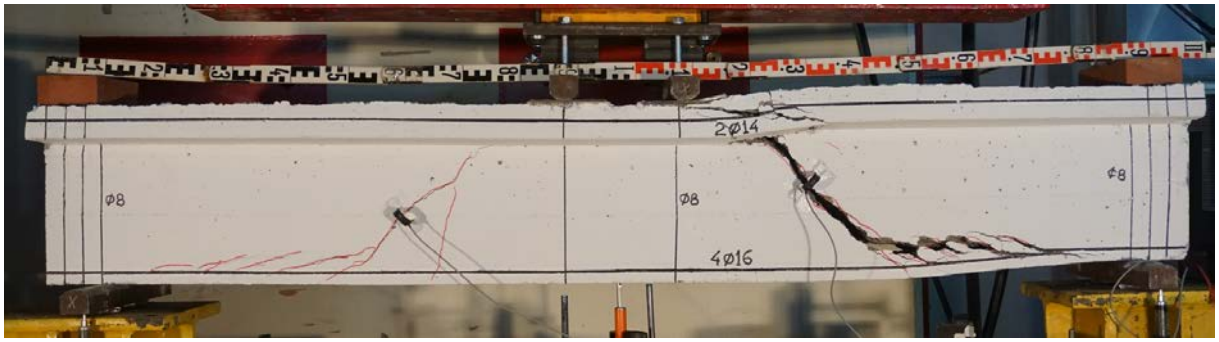

Figure 5: S0 specimen's mode of failure.

The S0-U specimen, which was strengthened using EB-FRP sheet strips, exhibited an initial response equivalent to the reference specimen. As the load increased, flexural cracks formed in the middle span and shear spans, with their length increasing progressively. In the two shear spans, the first shear cracks appeared. The shear fracture occurred between the FRP sheets in the middle and leading to a slight loss of strength. Subsequently, a second shear crack developed at the intersection of the left shear span and the left end sheet as the load increased. Debonding of the end FRP sheet started in the right shear span at a load of 176 kN, resulting in a rapid widening of the intersecting crack that eventually spread into the slab region and resulted in beam failure (Figure 6).

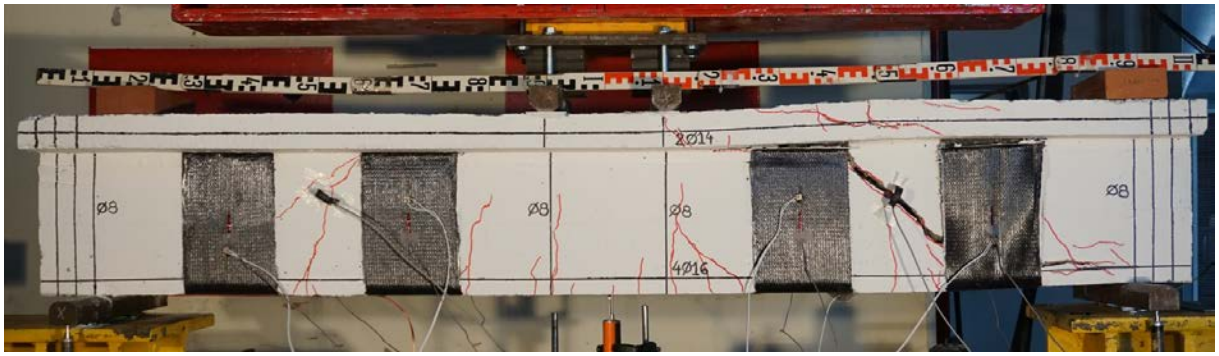

Figure 6: S0-U specimen's mode of failure.

The S0-RF specimen, which was strengthened with FRP ropes, exhibited similar early behavior to the other specimens. After the short elastic phase, the first flexural cracks appeared in the beam's middle region and then in the shear spans. In contrast to the other two specimens, an increase in the imposed displacement led to the formation of dense shear cracks with a narrow width in the two shear spans. The yielding of the tensile reinforcement occurred at a load of 308 kN. After the tensile reinforcement yielded, a further increase in the imposed displacement resulted in the gradual widening of the flexural cracks without, however, a substantial reduction in the strength of the beam (plastic behavior) (Figure 7).

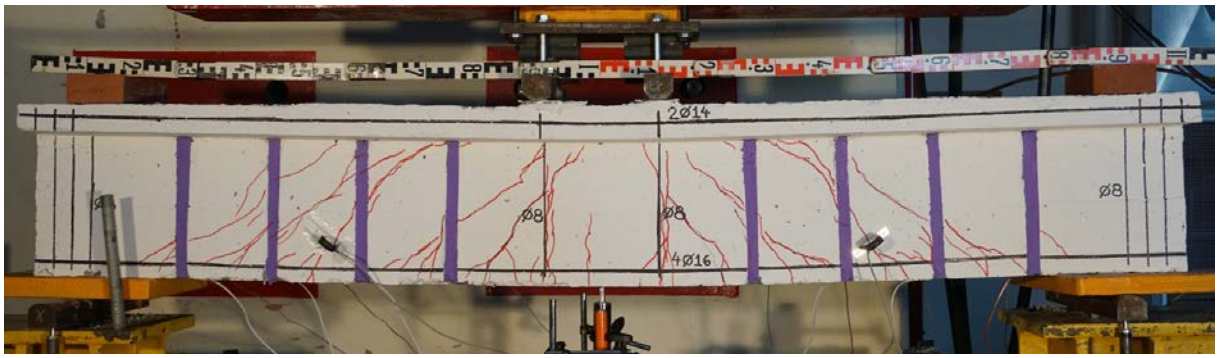

Figure 7: S0-RF specimen's mode of failure.

In order to gain a better understanding of the behavior of the beams, a load-deflection diagram at the mid-span of each beam was presented in Figure 8. The behavior of all three beams was linear-like until the formation of the first shear cracks. The reference specimens exhibited brittle failure due to the initiation and propagation of shear cracks. The application of FRP sheets in the shear spans of beam S0-U resulted in an increase in the ultimate load and improved the shear strength of the specimen. However, the load-bearing capacity decreased rapidly after debonding of the FRP sheet, ultimately leading to beam failure.

The application of FRP ropes utilizing the NSM technique, involving complete wrapping of the specimens' cross-section, resulted in a significant enhancement in strength. Notably, this strengthening method induced an alteration in the failure mode of the beam from the brittle shear mode to the desired ductile flexural mode.

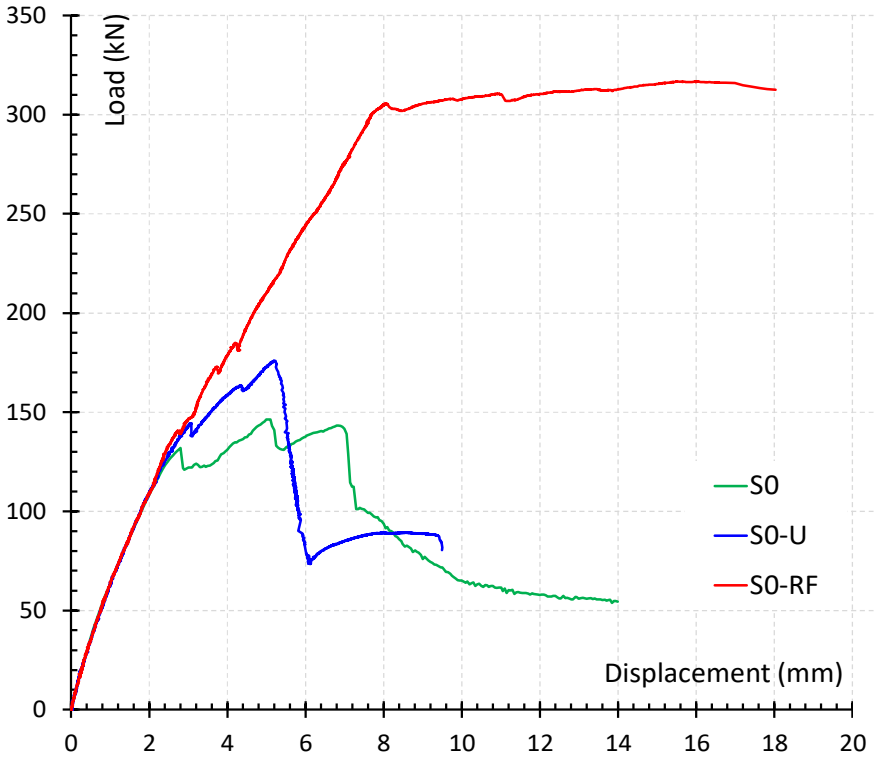

Figure 8: Diagram of imposed force versus deflection in the middle of each beam.

3.2 PZT Results

The WiAMS system uses the EMI method to measure each PZT patch electromechanical signature. Therefore, it is feasible to convert the variations in EMI signatures from the pristine to any subsequent condition to damage index metrics through statistical analysis of the EMI signatures. The Root Mean Square Deviation (RMSD) was employed to analyze the EMI signatures in this work. The expression of the RMSD scalar index is also presented in Equation (1).

$$\mathrm{RMSD} = \sqrt{\frac{\sum_1^N (|V_P(\omega)|_D - |V_P(\omega)|_0)^2}{\sum_1^N (|V_P(\omega)|_0)^2}} \tag{1}$$

where: $|V_P(\omega)|_D$, $|V_P(\omega)|_0$ are PZT's absolute value of peak voltage signals measured at pristine conditions (healthy state) and multiple damage levels (Dam1, Dam2, …, Dam5), respectively, and N is the number of discrete frequency measurements.

As explained earlier, RMSD values can quantify discrepancies between PZT signatures measured by WiAMS at different damage levels. The results of the RMSD indices for PZTS incorporated into the S0-U specimen can be seen in Figure 9. Until Dam 3, insignificant dispersed cracking was detected in FRP sheets without indications that the bonding had degraded. All PZTs at the prior damage states showed minor RMSD values.

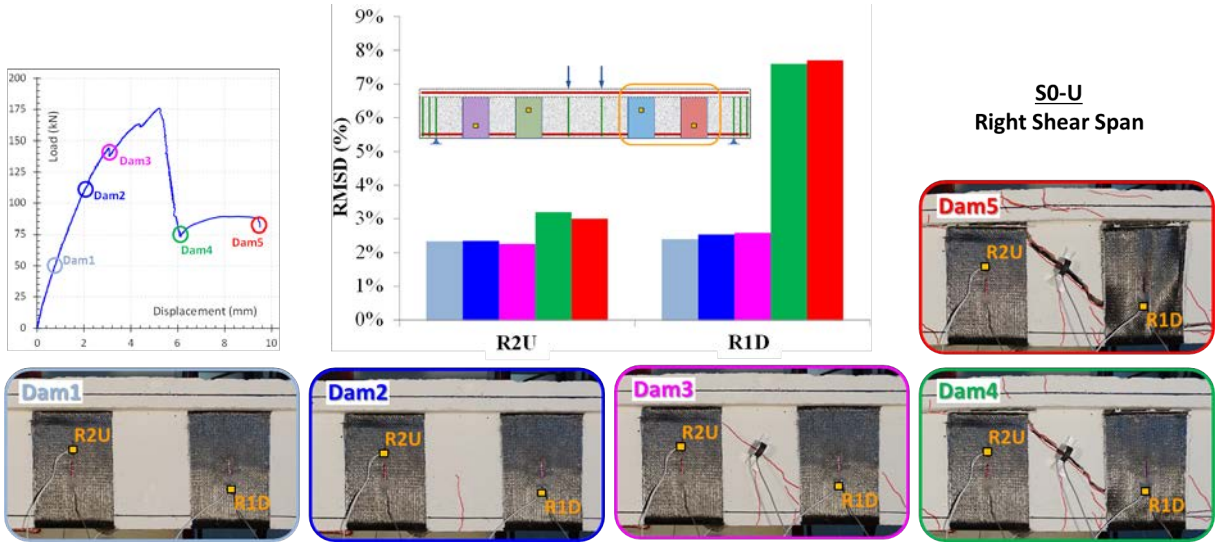

(a)

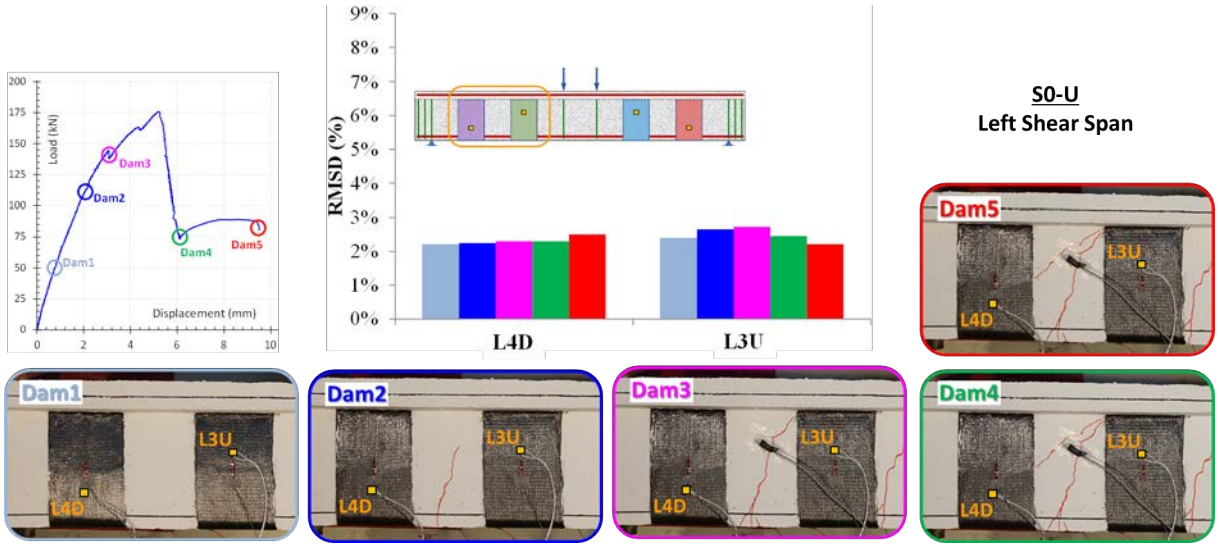

(b)

Figure 9. RMSD index values of PZT used in S0-U specimen: (a) “R2U” and “R1D” and (b) “L3U” and “L4D”.

At higher damage states (Dam4 and Dam 5), PZTs mounted to the right shear span ("RE" and "RI"), however, show significant increases in RMSD index values compared to PZTs mounted to the left shear span ("RE" and "RI"). This is due to the formation of the fatal crack in the right shear span of S0-U. The RMSD value of PZT "RE" has increased dramatically as a result of the debonding of the FRP sheet on which it was mounted. Therefore, PZTs' efficacy in identifying debonding of FRP sheets is established.

Specimen S0-RF, which was reinforced with externally bonded FRP ropes, has four epoxy-bonded PZT patches mounded on the FRP ropes on the lower surface of the specimen. The RMSD values of all PZTs exhibit a slight increase until Dam3 due to crack formation leading to stress development in the external reinforcement. Reaching the specimen's flexural load-bearing capacity leads to widening the flexural crack. In contrast, shear cracks remain stable thanks to the FRP ropes, despite the increase in the imposed deformation in the midspan of the specimen.

In contrast to specimen S0-U, all the FRP ropes were appropriately performed as shear reinforcement without signs of bonding degradation. This explains the insignificant RMSD values of PZTs of specimen S0-RF in all damage stages (Figure 10). These results show that debonding of externally bonded FRP is accompanied by vigorous growth in RMSD values.

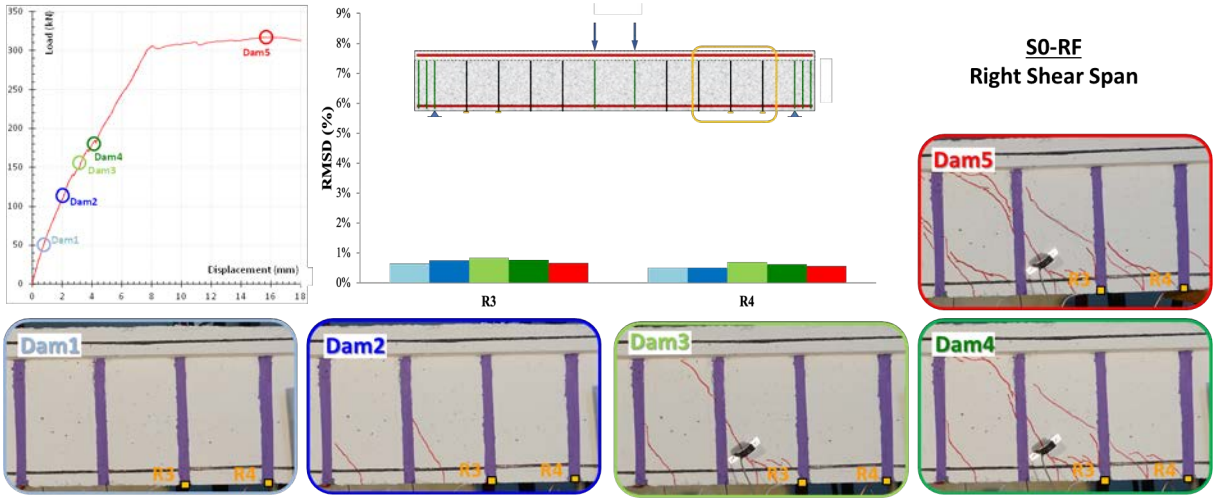

(a)

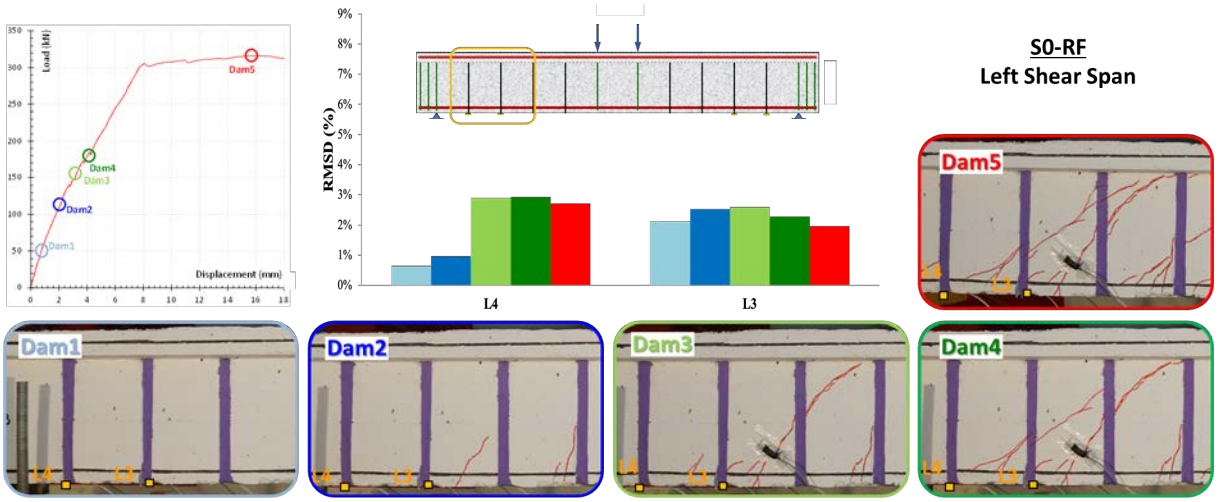

(b)

Figure 10. RMSD index values of PZT used in S0-RF specimen: (a) “R3” and “R4” and (b) “L4” and “L3”.

4 CONCLUDING REMARKS

The current study presented an experimental investigation of shear-critical RC beams retrofitted using carbon FRPs. Three large-scale beams with T-shape cross section were tested. One of the beams was the reference specimen, while the other two were strengthened against shear using EB-FRP sheets and FRP ropes with NSM respectively. The experimental response of the specimens was presented in terms of load – deflection diagrams and the efficiency of each strengthening technique was discussed. Further, a novel wireless SHM system with smart PZT sensors was used during testing to monitor and detect potential damages due to debonding of the FRP materials. Based on the results of this experimental study the following conclusions were drawn.

- The strengthening method using EB-FRP sheets enhances the beam's shear resistance in comparison to the reference specimen. Nevertheless, the debonding of the FRP sheet prevents the complete utilization of its strength, thereby leading to the beam's shear failure.
- The use of FRP ropes as NSM – ETS strengthening against shear is a very effective and promising technique. The application of this method not only led to a significant en-

hancement of the shear strength of the specimen but also to alteration of the mode of failure from shear to flexure.

- The proposed method using FRP ropes is easy and efficient to implement, and it involves minimal intervention in the surrounding slab area.
- The employed SHM system effectively detects the debonding of FRP sheets and accurately identifies the debonded region. When FRP ropes were utilized for strengthening, the SHM system did not exhibit any substantial signal variations that could indicate damage to the FRP material, consistent with the experimental findings. The shear strengthening approach using FRP ropes was successful, as the beam failure occurred due to flexure and not due to debonding or damage to the FRP ropes, which was also verified by the data gathered from the implemented PZT sensors.

ACKNOWLEDGMENTS - FUNDING:

The authors also acknowledge support of this work by the project "Risk and Resilience Assessment Center—Prefecture of East Macedonia and Thrace-Greece." (MIS 5047293) which is implemented under the Action "Reinforcement of the Research and Innovation Infrastructure", funded by the Operational Programme "Competitiveness, Entrepreneurship and Innovation" (NSRF 2014–2020) and co-financed by Greece and the European Union (European Regional Development Fund). Author Adamantis G. Zapris gratefully acknowledges the financial support received from Eugenides Foundation towards doctoral studies.

REFERENCES

1. Y. Zhou, J. Zhang, W. Li, B. Hu, X. Huang, Reliability-based design analysis of FRP shear strengthened reinforced concrete beams considering different FRP configurations, *Composite Structures*, **237**, 111957, 2020. doi: 10.1016/j.compstruct.2020.111957.
2. A. Siddika, Md. A. A. Mamun, R. Alyousef, Y. H. M. Amran, Strengthening of reinforced concrete beams by using fiber-reinforced polymer composites: A review, *Journal of Building Engineering*, **25**,100798, 2019. doi: 10.1016/j.jobe.2019.100798.
3. E. Moradi, H. Naderpour, A. Kheyroddin, An experimental approach for shear strengthening of RC beams using a proposed technique by embedded through-section FRP sheets, *Composite Structures*, **238**, 111988, 2020. doi: 10.1016/j.compstruct.2020.111988.
4. Y. Zhou, L. Sui, X. Huang, M. Guo, M. Luo, B. Hu, C. Chen, Enhancing the EB-FRP strengthening effectiveness by incorporating a cracking-control layer of ECC with different thicknesses, *Construction and Building Materials*, **286**, 122975, 2021. doi: 10.1016/j.conbuildmat.2021.122975.
5. C. E. Chalioris, A. G. Zapris, C. G. Karayannis, U-Jacketing Applications of Fiber-Reinforced Polymers in Reinforced Concrete T-Beams against Shear—Tests and Design, *Fibers*, **8**(2), 3, 2020. doi: 10.3390/fib8020013.
6. C. Yuan, W. Chen, T. M. Pham, H. Hao, Bond behaviour between hybrid fiber reinforced polymer sheets and concrete, *Construction and Building Materials*, **210**, 93–110, 2019. doi: 10.1016/j.conbuildmat.2019.03.082.
7. M. R. Irshidat, M. H. Al-Saleh, Effect of using carbon nanotube modified epoxy on bond–slip behavior between concrete and FRP sheets, *Construction and Building Materials*, **105**, 511–518, 2016. doi: 10.1016/j.conbuildmat.2015.12.183.

8. R. Kotynia, E. Oller, A. Marí, and M. Kaszubska, Efficiency of shear strengthening of RC beams with externally bonded FRP materials – State-of-the-art in the experimental tests, *Composite Structures*, **267**, 113891, 2021. doi: 10.1016/j.compstruct.2021.113891.
9. A. Godat, F. Hammad, O. Chaallal, State-of-the-art review of anchored FRP shear-strengthened RC beams: A study of influencing factors, *Composite Structures*, **254**, 112767, 2020. doi: 10.1016/j.compstruct.2020.112767.
10. E. Kaya, C. Kütan, S. Sheikh, and A. İlki, Flexural Retrofit of Support Regions of Reinforced Concrete Beams with Anchored FRP Ropes Using NSM and ETS Methods under Reversed Cyclic Loading, *J. Compos. Constr.*, **21**(1), 04016072, 2017. doi: 10.1061/(ASCE)CC.1943-5614.0000732.
11. G. Al-Bayati, R. Al-Mahaidi, R. Kalfat, Torsional strengthening of reinforced concrete beams using different configurations of NSM FRP with epoxy resins and cement-based adhesives, *Composite Structures*, **168**, 569–581, 2017. doi: 10.1016/j.compstruct.2016.12.045.
12. E. Golias, A.G. Zapris, V.K. Kytinou, M. Osman, M. Koumtzis, D. Siapera, C.E. Chalioris, C.G. Karayannis, Application of X-Shaped CFRP Ropes for Structural Upgrading of Reinforced Concrete Beam–Column Joints under Cyclic Loading–Experimental Study. *Fibers,* **9** (7), 42, 2021. https://doi.org/10.3390/fib9070042
13. E. Golias, A. G. Zapris, V. K. Kytinou, G. I. Kalogeropoulos, C. E. Chalioris, C. G. Karayannis, Effectiveness of the Novel Rehabilitation Method of Seismically Damaged RC Joints Using C-FRP Ropes and Comparison with Widely Applied Method Using C-FRP Sheets—Experimental Investigation, *Sustainability*, **13** (11), 6454, 2021. doi: 10.3390/su13116454.
14. C.G. Karayannis, E. Golias, G. I. Kalogeropoulos, Influence of Carbon Fiber-Reinforced Ropes Applied as External Diagonal Reinforcement on the Shear Deformation of RC Joints, *Fibers*, **10**(3), 28, 2022. doi: 10.3390/fib10030028.
15. C. G. Karayannis, E. Golias, Full-scale experimental testing of RC beam-column joints strengthened using CFRP ropes as external reinforcement, *Engineering Structures*, **250**, 113305, 2022. doi: https://doi.org/10.1016/j.engstruct.2021.113305.
16. M. Saadah, A. Ashteyat, and Y. Murad, Shear strengthening of RC beams using side near surface mounted CFRP ropes and strips, *Structures*, **32**, 380–390, 2021. doi: 10.1016/j.istruc.2021.03.038.
17. G. Markou, R. Garcia, C. Mourlas, M. Guadagnini, K. Pilakoutas, M. Papadrakakis, A new damage factor for seismic assessment of deficient bare and FRP-retrofitted RC structures, *Engineering Structures*, **248**, 113152, 2021. doi: 10.1016/j.engstruct.2021.113152.
18. O. Ahmed, X. Wang, M.-V. Tran, M.-Z. Ismadi, Advancements in fiber-reinforced polymer composite materials damage detection methods: Towards achieving energy-efficient SHM systems, *Composites Part B: Engineering*, **223**, 109136, 2021. doi: 10.1016/j.compositesb.2021.109136.
19. D. Li, J. Zhou, J. Ou, Damage, nondestructive evaluation and rehabilitation of FRP composite-RC structure: A review, *Construction and Building Materials*, **271**, 121551, 2021. doi: 10.1016/j.conbuildmat.2020.121551.
20. R. Perera, L. Torres, A. Ruiz, C. Barris, and M. Baena, An EMI-Based Clustering for Structural Health Monitoring of NSM FRP Strengthening Systems, *Sensors*, **19**(17), 3775, 2019. doi: 10.3390/s19173775.
21. R. Perera, E. Sevillano, A. Arteaga, A. De Diego, Identification of intermediate debonding damage in FRP-plated RC beams based on multi-objective particle swarm

optimization without updated baseline model, *Composites Part B: Engineering*, **62**, p205–217, 2014. doi: 10.1016/j.compositesb.2014.02.008.

22. A. G. Zapris, M. C. Naoum, V. K. Kytinou, G. M. Sapidis, and C. E. Chalioris, Fiber Reinforced Polymer Debonding Failure Identification Using Smart Materials in Strengthened T-Shaped Reinforced Concrete Beams, *Polymers*, **15**(2), 278, 2023. doi: 10.3390/polym15020278.
23. C. G. Karayannis, E. Golias, M. C. Naoum, C. E. Chalioris, Efficacy and Damage Diagnosis of Reinforced Concrete Columns and Joints Strengthened with FRP Ropes Using Piezoelectric Transducers, *Sensors*, **22**(21), 8294, 2022. doi: 10.3390/s22218294.
24. N. A. Papadopoulos, M. C. Naoum, G. M. Sapidis, and C. E. Chalioris, Cracking and Fiber Debonding Identification of Concrete Deep Beams Reinforced with C-FRP Ropes against Shear Using a Real-Time Monitoring System, *Polymers*, **15**(3), 473, 2023. doi: 10.3390/polym15030473.
25. Chalioris Constantin E., Voutetaki Maristella E., and Liolios Angelos A., Structural health monitoring of seismically vulnerable RC frames under lateral cyclic loading, *Earthquakes and Structures*, **19**(1), 29–44, 2020. doi: 10.12989/EAS.2020.19.1.29.
26. E. Sevillano, R. Sun, and R. Perera, Damage Detection Based on Power Dissipation Measured with PZT Sensors through the Combination of Electro-Mechanical Impedances and Guided Waves, *Sensors*, **16**(5), 639, 2016. doi: 10.3390/s16050639.
27. C. E. Chalioris, V. K. Kytinou, M. E. Voutetaki, C. G. Karayannis, Flexural Damage Diagnosis in Reinforced Concrete Beams Using a Wireless Admittance Monitoring System—Tests and Finite Element Analysis, *Sensors*, **21**(3), 679, 2021. doi: 10.3390/s21030679.
28. M. E. Voutetaki, M. C. Naoum, N. A. Papadopoulos, G. Sapidis, and C. E. Chalioris, Cracking Diagnosis in Fibre Reinforced Concrete Cubes and Cylinders with Synthetic Fibres using a PZT-based Health Monitoring System, *Sch J Eng Tech*, **9**(9), 140–151, 2021. doi: 10.36347/sjet.2021.v09i09.004.
29. M. E. Voutetaki, M. C. Naoum, N. A. Papadopoulos, and C. E. Chalioris, Cracking Diagnosis in Fiber-Reinforced Concrete with Synthetic Fibers Using Piezoelectric Transducers, *Fibers*, **10**(1), 5, 2022. doi: 10.3390/fib10010005.